Human Bone Marrow Is Comprised of Adipocytes with Specific Lipid Metabolism

Camille Attané, David Estève, Karima Chaoui, Jason S. Iacovoni, Jill Corre, Mohamed Moutahir, Philippe Valet, Odile Schiltz, Nicolas Reina, Catherine Muller

Cell Reports

Human Bone Marrow Is Comprised of Adipocytes with Specific Lipid Metabolism

Graphical Abstract

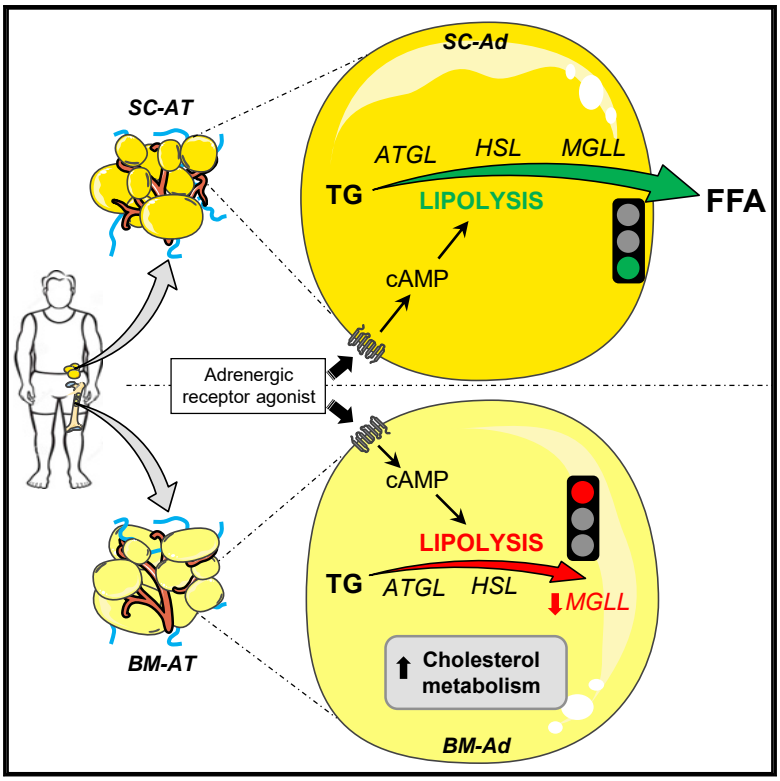

Highlights

- Like white adipocytes, BM-Ads contain a large lipid droplet filled with neutral lipids
- Lipolysis is altered in BM-Ads by a profound downregulation in expression of MGLL
- A defect in lipolysis explains why BM-Ads do not respond to caloric restriction
- BM-Ads exhibit a cholesterol-oriented metabolism

Authors

Camille Attané, David Estève, Karima Chaoui, ..., Odile Schiltz, Nicolas Reina, Catherine Muller

Correspondence

camille.attane@ipbs.fr (C.A.), muller@ipbs.fr (C.M.)

In Brief

Attané et al. show that, although human bone marrow adipocytes (BM-Ads) resemble classic white adipocytes on a morphological level, their lipid metabolism is highly specific. They are devoid of lipolytic activity, one of the main metabolic functions of white adipocytes, which explains why they behave like a preserved lipid source under energy-demanding conditions.

Attané et al., 2020, Cell Reports *30*, 949–958
January 28, 2020
https://doi.org/10.1016/j.celrep.2019.12.089

CellPress

Cell Reports
Report

Human Bone Marrow Is Comprised of Adipocytes with Specific Lipid Metabolism

Camille Attané,[1,7,*] David Estève,[1,7] Karima Chaoui,[1] Jason S. Iacovoni,[2] Jill Corre,[3] Mohamed Moutahir,[1] Philippe Valet,[4] Odile Schiltz,[1] Nicolas Reina,[5,6] and Catherine Muller[1,8,*]

[1]Institut de Pharmacologie et de Biologie Structurale (IPBS), Université de Toulouse, CNRS, UPS, Toulouse, France
[2]Plateau de Bioinformatiques, Institut des Maladies Métaboliques et Cardiovasculaires (I2MC), Université de Toulouse, INSERM, UPS, Toulouse, France
[3]Centre de Recherches en Cancérologie de Toulouse (CRCT), Université de Toulouse, INSERM, UPS, Toulouse, France
[4]Institut des Maladies Métaboliques et Cardiovasculaires (I2MC), Université de Toulouse, INSERM, UPS, Toulouse, France
[5]Département de Chirurgie Orthopédique et Traumatologique, Hôpital Pierre-Paul Riquet, CHU de Toulouse, Toulouse, France
[6]Laboratoire AMIS, UMR 5288 CNRS, Université Toulouse III-Paul Sabatier, Toulouse, France
[7]These authors contributed equally
[8]Lead Contact
*Correspondence: camille.attane@ipbs.fr (C.A.), muller@ipbs.fr (C.M.)
https://doi.org/10.1016/j.celrep.2019.12.089

SUMMARY

Under caloric restriction, bone marrow adipocytes (BM-Ads) do not decrease in size compared to white adipocytes, suggesting they harbor unique metabolic properties. We compare human primary BM-Ads with paired subcutaneous adipocytes (SC-Ads) using proteomic and lipidomic approaches. We find that, although SC-Ads and BM-Ads share similar morphological features, they possess distinct lipid metabolism. Although BM-Ad shows enrichment in proteins involved in cholesterol metabolism, correlating with increased free cholesterol content, proteins involved in lipolysis were downregulated. In particular, monoacylglycerol lipase expression is strongly reduced in BM-Ads, leading to monoacylglycerol accumulation. Consequently, basal and induced lipolytic responses are absent in BM-Ads, affirming their differences in metabolic fitness upon caloric restriction. These specific metabolic features are not recapitulated *in vitro* using common protocols to differentiate bone marrow mesenchymal stem cells. Thus, contrary to classical SC-Ads, BM-Ads display a specific lipid metabolism, as they are devoid of lipolytic activity and exhibit a cholesterol-orientated metabolism.

INTRODUCTION

In mammals, white adipose tissue (WAT) accumulates at various sites throughout the body. The most important and well-studied fat deposits occur in subcutaneous regions (SC-AT) and in the abdominal cavity surrounding key internal organs, such as the pancreas and intestines (Zwick et al., 2018). Other adipose-specific deposits form around the heart and kidneys, as well as the male prostate and female mammary glands (Zwick et al., 2018). In addition to WAT, mammals also possess brown adipose tissue (BAT) within the interscapular and supraclavicular regions, representing less than 5% of the total fat mass (Nedergaard et al., 2007; Leitner et al., 2017). Brown adipocytes participate in non-shivering thermogenesis and possess a specific morphology that includes several small lipid droplets and high mitochondrial content (Bartelt and Heeren, 2014). In contrast, white adipocytes store energy as triacylglycerol (TGs) in their single large lipid droplet (LD) after energy intake and release free fatty acids (FFAs) through lipolysis under energy-demanding conditions (Zechner, 2015). Lipolysis occurs through a biochemical pathway that employs the consecutive actions of adipose triglyceride lipase (ATGL), catalyzing the conversion of TGs to diacylglycerols (DGs) and hormone-sensitive lipase (HSL) (encoded by the LIPE gene), hydrolyzing DGs to monoacylglycerols (MGs) and monoacylglycerol lipase (MGLL), as well as the newly identified α/β hydrolase domain-containing protein 6 (ABHD6) (Zhao et al., 2016), hydrolyzing MGs to FFAs and glycerol (Zechner, 2015). White adipocytes also have an important endocrine function, as they release multiple soluble factors called adipokines, such as leptin and adiponectin (Fasshauer and Blüher, 2015).

Bone marrow adipose tissue (BM-AT) represents an intriguing form of AT that constitutes over 10% of the total fat mass in lean and healthy humans (Cawthorn et al., 2014). Technological advances in quantitative imaging of BM-AT in both mice and humans revealed that BM-AT presents unique features that highlight their physiological specificity. Many studies have demonstrated that BM-AT increases with various pathophysiological conditions, such as aging (Justesen et al., 2001; Scheller et al., 2015), osteoporosis (Justesen et al., 2001; Yeung et al., 2005), and obesity (Bredella et al., 2011; Doucette et al., 2015). These findings suggest that bone marrow adipocytes (BM-Ads) play a more significant role than merely being space-filler cells. In stark contrast to other types of WAT, caloric restriction conditions lead to an increase in the number and size of BM-Ads in mice (Cawthorn et al., 2014; Devlin et al., 2010), rabbits (Bathija et al., 1979;

Tavassoli, 1974), and human patients suffering from anorexia nervosa (Abella et al., 2002; Bredella et al., 2011). Conversely, a decrease in bone marrow adiposity only occurs during severe nutrient deprivation in rabbits (Cawthorn et al., 2016) and late stages of anorexia nervosa, associated with gelatinous transformation of the bone marrow (BM) (Abella et al., 2002; for review, Ghali et al., 2016).

Given the significant role for AT in regulating energy homeostasis, it is critical to elucidate why BM-AT copes with changes in energy status in such a specific way, leading to stocking and not dispensing fuel when needed. However, physiological information regarding the phenotype of primary BM-Ads is limited, hampered by the difficulties inherent to the obtention of sufficient numbers of isolated BM-Ads from mice as well as issues related to harvesting human BM-AT, partly due to its physical location inside bone. Thus, most studies on BM-Ads use rodent or human *in vitro* models. Mouse studies indicate that BM-Ad regulates hematopoiesis and bone mass (Naveiras et al., 2009; Zhou et al., 2017). However, the existence of species-specific differences between rodent and human BM-AT reinforces the use of caution when extrapolating information across species (Scheller et al., 2016). Two types of murine BM-Ads have been described: regulatory and constitutive BM-Ads (rBM-Ads and cBM-Ads, respectively; Scheller et al., 2015). cBM-Ads are present in tail vertebrae and the medullary canal from the tibia-fibula junction of the malleolus. However, rBM-Ads develop postnatally within the BM of long bones extending from below the growth plate through the metaphysis and into the diaphysis (Scheller and Rosen, 2014). Existence of these two populations remains unconfirmed in humans. Inside the long bone diaphysis, the number of BM-Ads varies between mouse strains and species. Some strains require pharmacological induction of BM-Ads by drugs, such as glucocorticoids and thiazolidinedione (Scheller et al., 2016). Yet human BM-Ad consistently fills 50%–70% of the bone marrow cavity (Hindorf et al., 2010). Many studies use bone marrow mesenchymal stromal cells (BM-MSCs) differentiated into adipocytes *in vitro*. However, it is unclear whether these differentiated cells recapitulate the phenotype of mature human primary BM-Ads. These *in vitro* studies suggest a role for BM-Ads in hematopoiesis regulation (Mattiucci et al., 2018; Naveiras et al., 2009), bone remodeling (Hardaway et al., 2015), and cancer progression (Diedrich et al., 2016; Herroon et al., 2013; Liu et al., 2015; Shafat et al., 2017; Tabe et al., 2017). Taken together, there exist a number of issues that highlight that our knowledge of the physiological phenotype of primary BM-Ad remains limited. We have purified human BM-Ads harvested from the femoral diaphysis of patients undergoing hip surgery alongside paired subcutaneous adipocytes (SC-Ads). Using a combination of proteomic and lipidomic approaches, we found that BM-Ad clearly exhibits distinct lipid metabolic features compared to white adipocytes.

RESULTS AND DISCUSSION

Isolated BM-Ads Share Morphological Properties with White SC-Ads

Paired SC-AT and BM-AT were harvested from patients undergoing hip replacement surgery, and adipocytes were isolated using collagenase digestion (Figure 1A). In AT from both locations, the vast majority of the space contained large and cohesive mature adipocytes with a unique LD filled with neutral lipids (assessed by Bodipy staining; Figure 1B). Mature adipocytes from both locations expressed Perilipin 1 (PLIN1) at the surface of the LD (Figures S1A and S1B) and exhibited a very thin cytoplasmic rim, a morphological trait of white adipocytes (Figure S1B; Cinti, 2001). SC-AT and BM-AT also contained blood vessels highly positive for actin staining and stroma vascular cells in both stromal and perivascular positions (Figures 1B and S1A). Using transmission electron microscopy, we observed that both SC-Ads and BM-Ads display a large LD surrounded by a very thin cytoplasm, with the nucleus located at the cell periphery (Figure 1C). We performed an enzymatically based digestion protocol to isolate adipocytes from both tissues. After obtaining a population of cells consisting of only adipocytes, we confirmed that our tissue dissociation preserved the morphological identity of the isolated adipocytes. Isolated BM-Ads and SC-Ads shared the same morphology found within the tissues, characterized by the presence of a unique and large LD filled with neutral lipids (Figure 1D). In addition, F-actin staining showed a similar cytoskeletal architecture between the two cell types (Figure 1D). As shown in Figures S1C and S1D, the size of isolated BM-Ads was not different from that of SC-Ads (mean diameter of 95 ± 6 μm for SC-Ads and 90 ± 7 μm for BM-Ads). Taken together, our results demonstrate that the BM-AT, present in the long bone diaphysis, is composed of cohesive adipocytes that exhibit a morphological appearance akin to that of white adipocytes, as assessed by their unique LD, which is surrounded by a thin cytoplasm and a nucleus at the cell periphery. As noted in the introduction, a recent study in mice using transmission electron microscopy found that BM-Ads exhibit a similar rounded morphology with a single large LD (Robles et al., 2019). Yet another report suggested that murine BM-Ads express some genes related to BAT, including PRDM16 and FOXC2 (Krings et al., 2012). However, this study used whole tibia extracts, containing adipocytes as well as contaminates, including myeloid cells and osteoblasts that express PRDM16 and FOXC2, respectively (Kim et al., 2009; Nishikata et al., 2011). Here, we present an initial morphological characterization of human BM-Ads as being indistinguishable from ''classical'' white adipocytes.

Proteomes of BM-Ads and SC-Ads Differentiate Their Lipid Metabolic Functions

To better understand the metabolic specificities of BM-Ads, we conducted proteomic analyses on paired SC-Ads and BM-Ads. The general data analysis strategy is described in Figure S2A. After quality control, 3,259 proteins were robustly detected. Interestingly, when we searched for proteins known to be secreted by adipocytes, termed adipokines (Fasshauer and Blüher, 2015), our dataset did not highlight significant differences between the two types of adipocytes. Furthermore, k-means clustering of adipokine expression did not partition samples according to their anatomical location (Figure S2B). As shown in Table S1, BM-Ads and SC-Ads expressed similar levels of both the adipocyte-specific adipokine adiponectin (ADIPOQ), as well as leptin (LEP), a hormone predominantly produced by adipocytes (Fasshauer and Blüher, 2015).

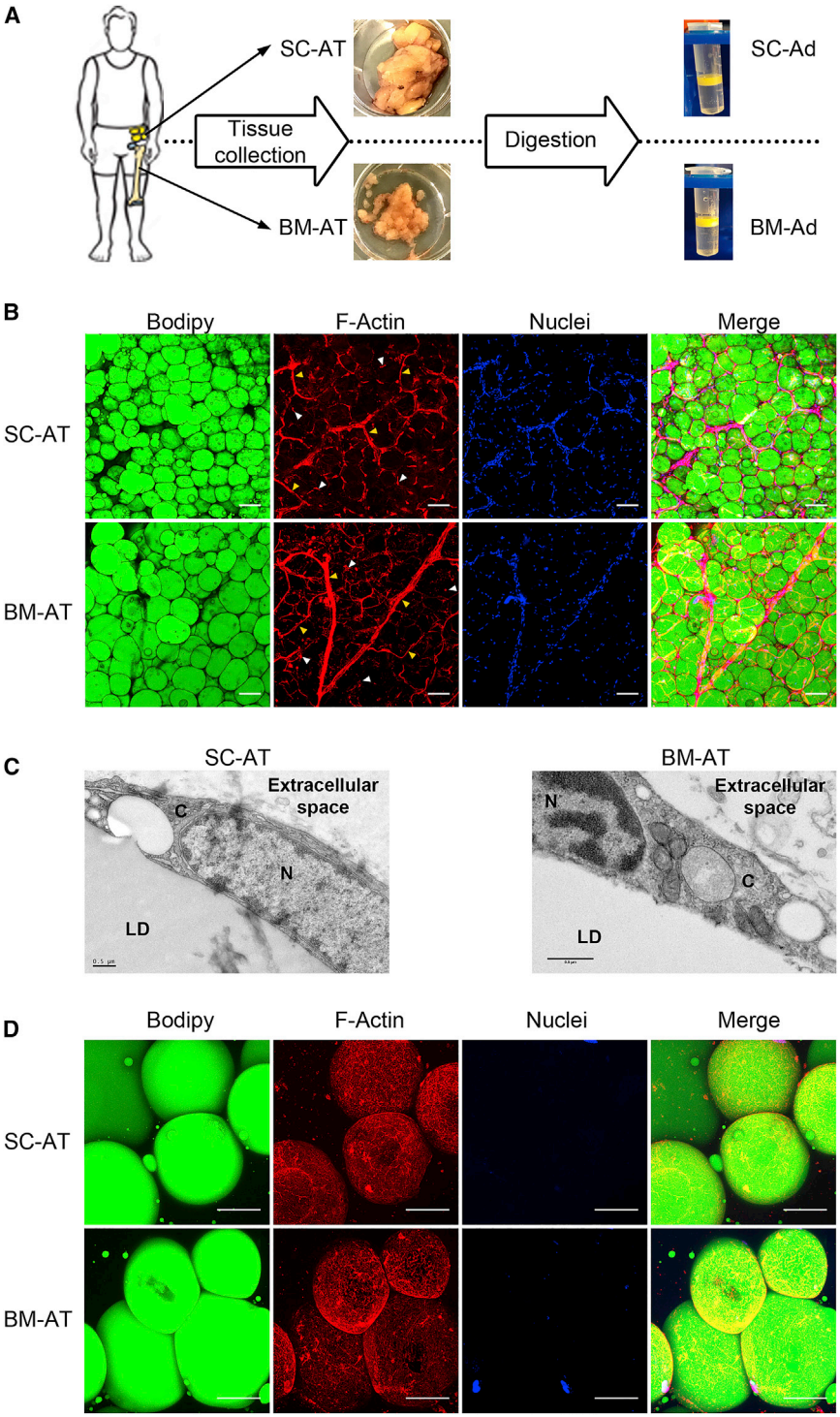

Figure 1. SC-Ads and BM-Ads Exhibit Similar Morphological Properties

(A) Experimental protocol designed to obtain paired human primary BM-Ads and SC-Ads.

(B) Whole-mount SC-ATs and BM-ATs were stained with Bodipy 493/503 (neutral lipids, green), phalloidin (F-actin, red), and TOPRO-3 (nuclei, blue). Representative maximum intensity projection of z stack images is shown (n = 3; objective 10×). Orange arrowheads show vessels. White arrowheads show stromal cells. Scale bars, 100 μm.

(C) Transmission electron microscopy images of SC-ATs and BM-ATs. C, cytoplasm; LD, lipid droplet; N, nucleus. Scale bars, 0.5 μm.

(D) Primary SC-Ads and BM-Ads isolated and stained with Bodipy 493/503 (neutral lipids, green), phalloidin (F-actin, red), and TOPRO3 (nuclei, blue). Representative maximum intensity projection of z stack images is shown (n = 3; objective 40×). Scale bars, 50 μm.

See also Figure S1.

Among the 3,259 proteins detected, 612 proteins involved in glucose and lipid metabolism were identified. An unsupervised multivariate analysis with these proteins clearly partitioned the samples according to anatomical location (Figure 2A), with the first two components explaining 41% and 20.8% of the total variance (Figure 2A). Analysis of these 612 metabolic proteins identified 68 with greater expression in BM-Ads and 67 expressed more in SC-Ads (Figure 2B). Pathway enrichment analysis showed clear differences for several lipid metabolism pathways due to anatomical location (Figure 2C). Proteins with higher expression in BM-Ads enriched pathways for arachidonic acid (AA) metabolism (Figure S2C), sphingolipid (SL) signaling, and cholesterol metabolism (cholesterol biosynthesis and statin pathway). Proteins expressed at greater levels in SC-Ads enriched for pathways involved in glucose and FA metabolism (Figure S2D) as well as lipolysis regulation (Figure 2C). In-depth analysis of the lipolysis pathway showed that the lipases involved in TG hydrolysis, HSL, MGLL, and the lipid droplet protein PLIN1, were decreased, in addition to Fatty Acid Binding Protein 4 (FABP4), which represents one of the most abundant proteins of adipocytes that participate in both the maintenance of adipocyte homeostasis and the regulation lipolysis and adipogenesis (Prentice et al., 2019; Figures 2D and 2E; Table S1). Analysis of protein-protein interactions (PPIs) highlight that, among the lipolysis effectors, the expression of MGLL is one of the most downregulated proteins in BM-Ads. In addition, prostaglandin endoperoxide synthase 1 (PTGS1) was highly enriched in BM-Ads (Figures 2D and 2E). PTGS1 is involved in synthesis of prostaglandins, which were described to have antilipolytic activity (Lafontan and Langin, 2009). In contrast, proteins involved in the regulation of lipolysis, either

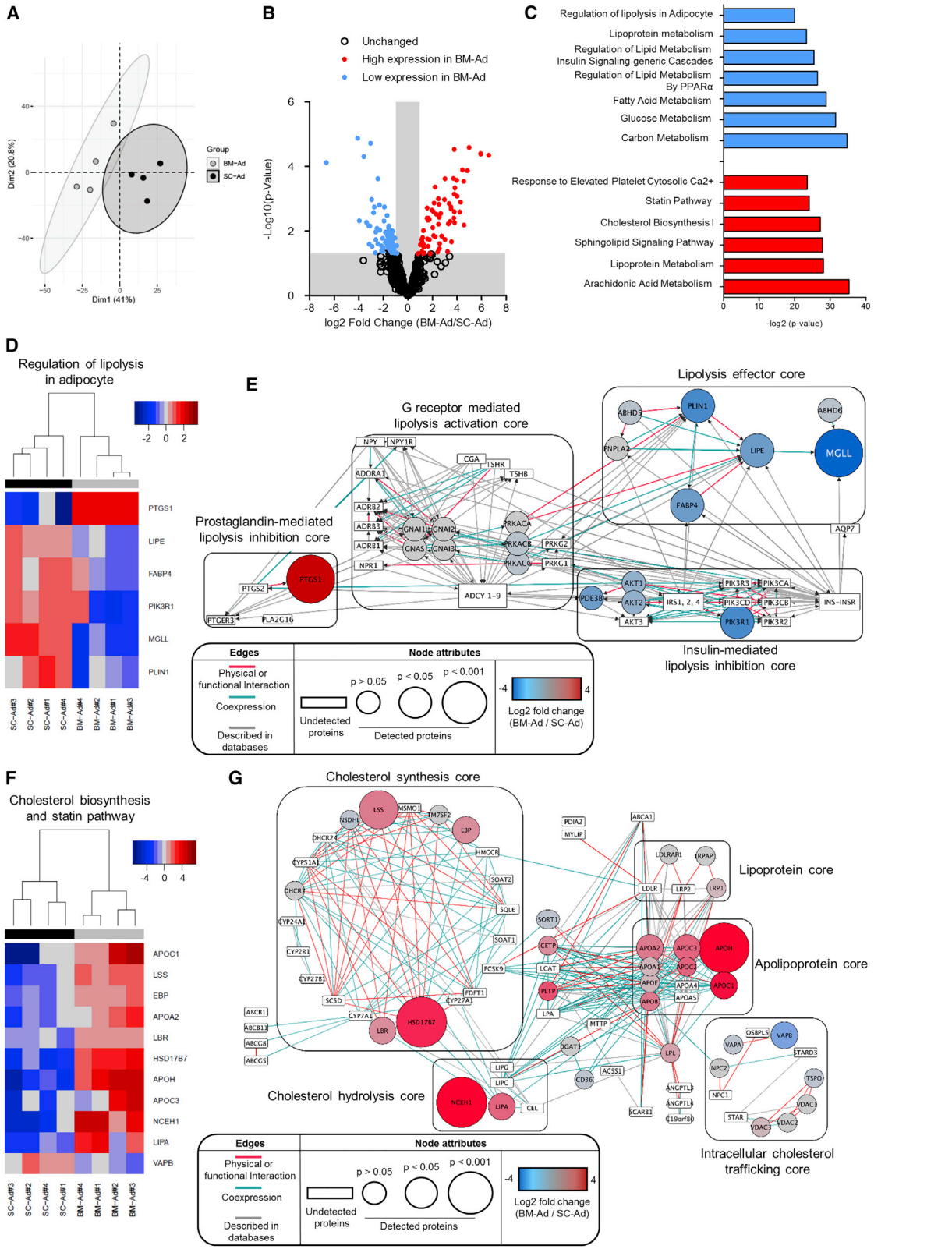

(legend on next page)

by insulin or G-coupled receptors, are expressed at similar levels in both BM-Ads and SC-Ads (Figure 2E). Taken together, these results highlight that BM-Ads present altered lipolytic function. Additionally, BM-Ads exhibit a cholesterol-oriented metabolism. Hierarchical clustering of differentially expressed cholesterol-related proteins clearly separated samples by location (Figure 2F). BM-Ad expresses proteins involved in cholesterol transport (apolipoproteins APO-A2, C1, C3, and H) and hydrolysis, such as NCEH1 (Neutral Cholesterol Ester Hydrolysis) and LIPA (Lipase A) (Litvinov et al., 2018), as well as proteins related to cholesterol synthesis, such as LSS (lanosterol synthase), EBP (emopamil-binding protein), LBR (lamin B receptor), and HSD17B7 (hydroxysteroid 17-beta dehydrogenase 7) (Figures 2F and 2G; Table S1). Although VAPB (VAMP Associated Protein B) was less expressed in BM-Ads, other proteins associated with cholesterol intracellular trafficking were not significantly modified with respect to SC-Ads (Figure 2G). Specific proteins from the lipoprotein metabolism pathway are either enriched or depleted in BM-Ads (Figure 2C), further strengthening the uniqueness of these cells in terms of lipid metabolism (Figure S2E). Indeed, proteins involved in cholesterol metabolism were expressed more in BM-Ads, and those involved in lipolysis were more expressed in SC-Ads (Figure S2G).

Despite sharing a similar morphology and expression profile for adipokines, our results strongly support the concept that BM-Ads are adipocytes exhibiting a very specific lipid metabolism compared to "classic" SC-Ads. A recent transcriptomic study comparing the gene expression of human SC-Ads and BM-Ads isolated from the femoral head showed that genes with higher expression in human BM-Ads participate in various signaling pathways. However, in contrast with our proteomic results, no differences in mRNA expression levels for enzymes involved in the lipolytic pathway (such as MGLL) and/or proteins involved in cholesterol metabolism were mentioned in this study (Mattiucci et al., 2018). In addition, this report found that adiponectin expression decreased in BM-Ads compared to SC-Ads, which conflicts with our findings as well as those from another study that identified BM-Ads as an important source of adiponectin (Cawthorn et al., 2014). Thus, we observe a discordance between mRNA and protein levels in this depot, as previously reported in other tissues (Vogel and Marcotte, 2012; Zhang et al., 2014).

Lipid Profile in BM-Ads Reveals Enriched Diverse Lipid Species, Like MG and Cholesterol

We then further characterize BM-Ads by studying their lipid profiles. Lipid content levels were indistinguishable when extracted from tissues and isolated adipocytes (Figures S3A and S3B). Quantitative liquid chromatography-tandem mass spectrometry (LC-MS/MS) of the total lipid content extracted from BM-Ads and SC-Ads was performed using a recently developed approach employing both positive and negative ionization modes to cover the largest spectrum of detectable lipid species (Breitkopf et al., 2017). This method structurally characterized and identified 818 lipid species from 15 different lipid classes and unsupervised multivariate analyses indicated the variance between samples predominantly arose through inter-individual variability (Figures S3C and S3D). The majority of identified lipid species found in both BM-Ads and SC-Ads were glycerolipids (GLs), including triacylglycerol (TG) (>90%) and DG (~2.5%), as well as phosphatidylcholine (PC), a major membrane constituent (Wen et al., 2018; Figure 3A). The remaining lipids mainly consisted of sphingolipids, other phospholipids (PL), as well as MG and fatty acid esters (Figure 3A). Quantified lipid species for each class were compared between BM-Ads and SC-Ads as shown in Figure 3B. We observed modifications in sphingolipids, with more sphingosine in BM-Ads and less ceramides and sphingomyelin when compared to SC-Ads. Finally, DG levels remain unchanged in BM-Ads, whereas TG and MG were increased. Both saturated and unsaturated MG species increased in BM-Ads (Figure 3C), suggesting that the hydrolysis of MG is not efficient in these cells. These results are consistent with the proteomic data showing that BM-Ads have a lower expression level of MGLL (Figure 2D), required for the final hydrolysis of MG (Zechner, 2015). As such, MGLL deficiency in mice leads to a concomitant increase in MG levels in AT (Taschler et al., 2011). The concomitant decrease of MGLL expression and increase in MG species strongly suggests that MG hydrolysis may be impaired in BM-Ads compared to SC-Ads.

The LC-MS/MS approach we used to quantify lipid species is unable to identify cholesterol, a key lipid contained in the adipocyte LD (Schreibman and Dell, 1975). Using a colorimetric assay, we found that BM-Ads showed a 1.5-fold increase in free cholesterol content, as compared to SC-Ads (Figure 3D), supporting the unbiased proteomic approaches indicating a seemingly unidentified cholesterol-oriented metabolism in BM-Ads. In contrast, the main function of adipocytes, liberating energy reserve stores as TG under times of energy demand, appears to be less important for BM-Ads compared to SC-Ads, consistent with the absence of a decrease in BM adiposity under energy deficit conditions (Bathija et al., 1979; Cawthorn et al., 2014; Devlin et al., 2010; Tavassoli, 1974).

Figure 2. Large-Scale Proteome Analysis Highlights Differences in Lipid Metabolism between BM-Ads and SC-Ads

(A) Principal-component analysis of BM-Ad and SC-Ad samples using expression levels of proteins involved in lipid and glucose metabolism. 95% confidence ellipses are shown.

(B) Volcano plot of the 612 proteins involved in lipid and glucose metabolism.

(C) Pathway enrichment analysis performed with Gene Analytics. The top pathways enriched in BM-Ads (red bars) and SC-Ads (blue bars) are presented.

(D and F) Heatmaps of scaled protein expression in BM-Ad and SC-Ad samples for genes belonging to the regulation of lipolysis in adipocytes (D) or cholesterol biosynthesis and statin pathways (F). Dendrograms represent hierarchical clustering of the samples.

(E and G) Interaction networks of proteins belonging to the regulation of lipolysis in adipocytes (E) or cholesterol biosynthesis and statin pathways (G). Nodes represent detected proteins (circle) and undetected proteins (square) by LC-MS/MS. The size of the circle is based on the p value of differentially detected proteins and is color-coded according to log2-fold change of protein expression in BM-Ads compared to SC-Ads. Edges represent protein-protein interactions with a combined score in string database above 0.8. Edges are colored based on the type of interaction, as indicated in the figure.

See also Figure S2.

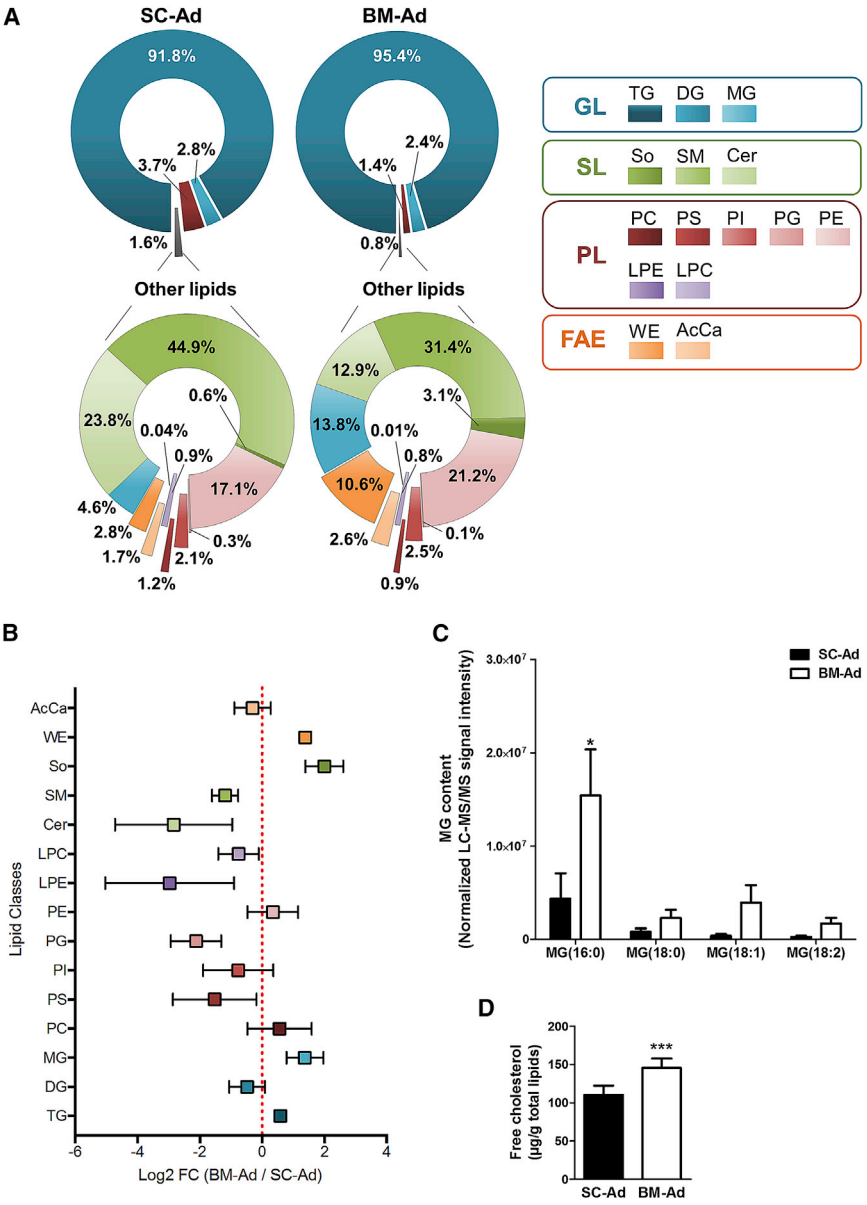

Figure 3. Lipid Profile of BM-Ad Reveals Enrichment of Diverse Lipid Species, Such as Monoacylglycerol (MG) and Cholesterol

(A) Pie charts of the mean relative abundance of the detected lipid classes using LC-MS/MS approach. The glycerolipids (GLs) are shown in shades of blue: triacylglycerol (TG); diacylglycerol (DG); and monoacylglycerol (MG). Sphingolipids (SLs) are in shades of green: sphingosine (So); sphingomyelin (SM), and ceramides (Cer). Phospholipids (PL) are in red and purple shades: phosphatidylcholine (PC); phosphatidylserine (PS); phostatidylinositol (PI); phosphatidylglycerol (PG); phosphatidylethanolamine (PE); lysophosphatidylethanolamine (LPE); and lysophosphatidylcholine (LPC). Fatty acid esters (FAE) are in shades of orange: wax ester (WE) and acyl carnitine (AcCa).

(B) Log2-fold change of the 15 lipid classes identified in BM-Ads compared to SC-Ads analyzed by LC-MS/MS (n = 4). The quantity of lipid classes was calculated as the sum of lipid species belonging to each class. The results represent the mean ± SEM.

(C) Relative quantification of the main MG species by LC-MS/MS in paired isolated SC-Ads and BM-Ads (n = 4). Histograms represent mean ± SEM; *$p < 0.05$ according to two-way ANOVA followed by Bonferroni's post-test.

(D) Free cholesterol content in BM-Ads and SC-Ads. The results were normalized to the total lipid quantity. The histograms represent mean ± SEM; ***$p < 0.001$ according to paired t test (n = 11). See also Figure S3.

Human Primary BM-Ads Present a Defect in Lipolytic Activity Not Recapitulated with *In Vitro* Models

Before performing functional characterization of the lipolysis pathway, we first checked the expression levels of the lipases involved in the consecutive hydrolysis of TG to glycerol (Figure 4A). Western blots revealed no major differences between BM-Ads and SC-Ads in terms of ATGL and HSL, despite the fact that we found a slight decrease in HSL protein expression in our proteomic studies. This discrepancy highlights inter-individual variability. Interestingly, we found a sharp decrease (about 5-fold) in MGLL in the three samples tested (Figure 4B), which is consistent with our proteomic results. Of note, two different forms of MGLL (between 35 and 40 kDa) were detected in BM-Ad samples, with an additional third form sometimes detected in SC-Ads (between 35 and 40 kDa), possibly resulting from differential start codon usage as well as alternative splicing, as previously described for other tissues (Karlsson et al., 2001; Nomura et al., 2010). Longer exposure times reveal that these two different forms of MGLL were also detected in the three BM-Ad samples (Figure S4A). These results largely confirmed that MGLL is the lipase with the largest difference in expression between SC-Ads and BM-Ads. In order to clearly establish a location-based functional difference in the lipolytic pathway, we performed *ex vivo* lipolysis assays on isolated adipocytes. Under basal conditions, we observed reduced glycerol and FFA release in BM-Ads compared to SC-Ads (Figures 4C and 4D). Upon stimulation with isoprenaline, a β-adrenergic agonist that serves as a strong lipolytic activator (Lafontan and Langin, 2009), we found that the expected increase in glycerol (reflecting complete lipolytic reactions) and FFA release were absent in BM-Ads. To confirm that this effect is not due to a defect in β-adrenergic receptor activation, we tested whether or not isoprenaline can activate adenylate cyclase in BM-AT and induce cyclic adenosine monophosphate (cAMP) production, which is upstream of lipolytic process. We found similar cAMP responses in both BM-AT and SC-AT (Figure 4E). Unlike SC-AT, direct activation of adenylate cyclase by forskolin failed to stimulate glycerol and FFA

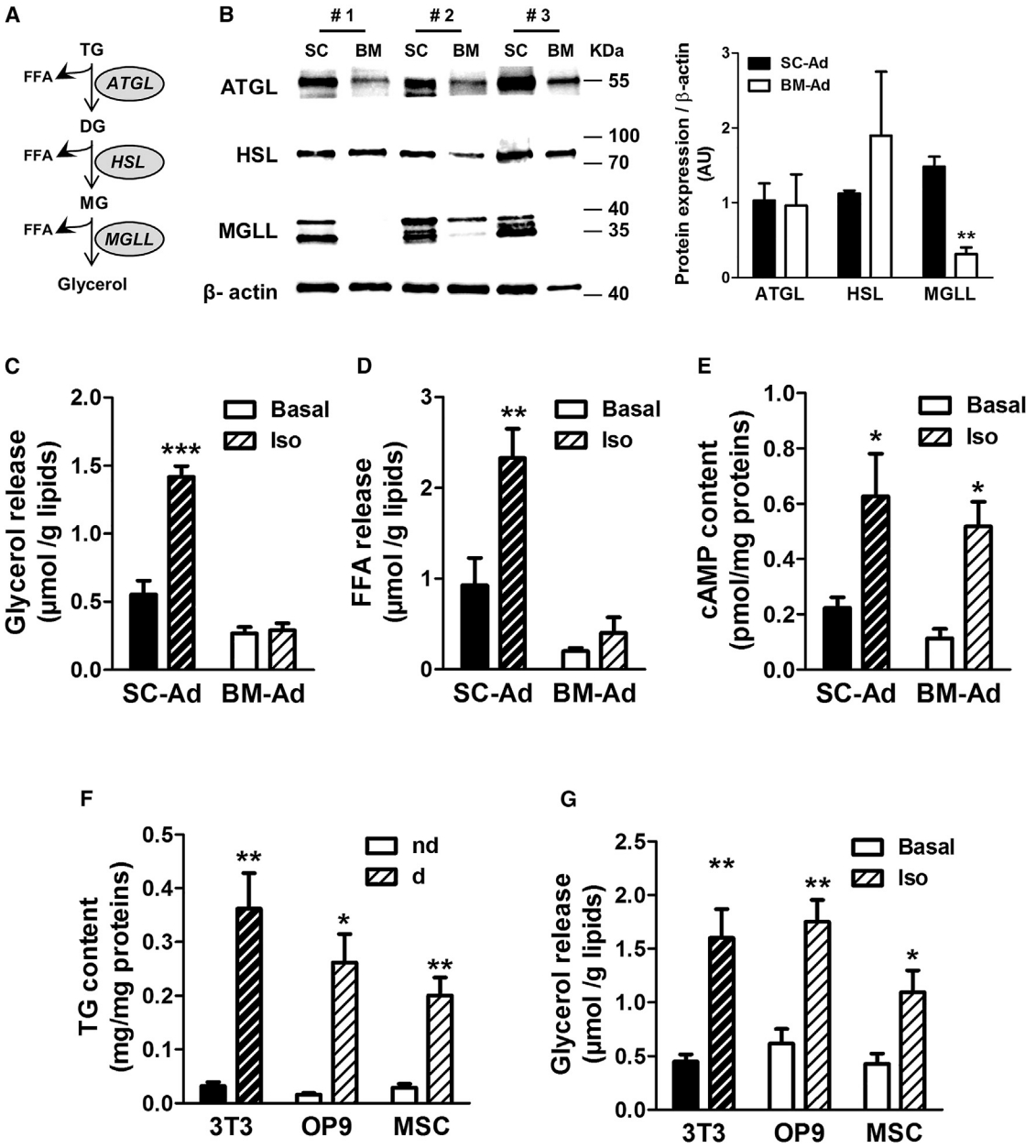

Figure 4. Human Primary BM-Ads Are Devoid of Lipolytic Activity, a Metabolic Trait Not Recapitulated by Primary BM-MSCs Differentiated *In Vitro*

(A) Scheme depicting the 3 steps of lipolysis and the lipases involved.

(B) Left panel: western blot analyses of the three main enzymes involved in lipolysis on paired isolated SC-Ads (SC) and BM-Ads (BM) from 3 independent donors. Right panel: relative quantifications of the band intensity normalized to the quantity of β-actin are shown. The histograms represent mean ± SEM. **$p < 0.01$ according to paired Student's t test.

(C) Glycerol release was measured from isolated SC-Ads and BM-Ads as a readout for complete lipolysis under basal conditions or after stimulation with isoprenaline (iso). The data are the means of 7 independent experiments and normalized to the total lipid quantity. The histograms represent mean ± SEM; ***$p < 0.001$ according to two-way ANOVA followed by Bonferroni post-test.

(D) Free fatty acids (FFAs) released from isolated SC-Ads and BM-Ads as a readout of lipolysis under basal conditions or after stimulation with isoprenaline. Data are the means of 7 independent experiments and are normalized to the total lipid quantity. The histograms represent mean ± SEM; **$p < 0.01$ according to two-way ANOVA followed by Bonferroni post-test.

(E) cAMP production in SC-AT and BM-AT after stimulation with isoprenaline for 30 min. Data are the mean of 8 independent experiments, normalized to protein content. Histograms represent the mean ± SEM; *$p < 0.05$ according to two-way ANOVA followed by Bonferroni post-test.

(F) TG content measured in cell lysates from 3T3F442A (3T3) and OP9 cell lines or human BM-MSCs (MSC) before and after adipogenic differentiation (d, differentiated; nd, non-differentiated). Data are the mean of at least 4 independent experiments (4 independent donors were used for human BM-MSCs) and

(legend continued on next page)

release in BM-AT, showing that lipolytic defect is downstream of adenylate cyclase (Figures S4B and S4C). Thus, our data clearly demonstrate that human BM-Ads are devoid of lipolytic activity, which is not due to a defect in β-adrenergic signaling but could be explained by the observed downregulation of MGLL.

We then examined whether or not this metabolic specificity is reproduced in *in vitro* differentiated BM-MSCs, a model largely used for studying the role of BM-Ads. We differentiated human primary BM-MSCs and murine BM-MSC OP9 cell lines *in vitro* under adipogenic conditions. The murine pre-adipocyte 3T3-F442A served as a control reflecting "classical adipocytes." The differentiation process strongly increased TG content (Figure 4E), and isoprenaline increased glycerol release in all cells studied (Figure 4F). These experiments demonstrated that human BM-MSCs-derived adipocytes do not recapitulate the functional defect in lipolysis observed in primary human BM-Ads. Thus, experiments done with these cells should be interpreted with caution, because they do not recapitulate the key metabolic trait of the BM-Ad phenotype. Previous experiments in mice have demonstrated that adipocyte progenitors from white and bone marrow adipocytes have common immunophenotype (CD45− CD31− Sca-1+ CD24−; Ambrosi et al., 2017). Although this point remains to be investigated in human cells, our results suggest that the distinctive features of BM-Ads could be due to differences in physiological conditions within the bone marrow that are not recapitulated by commonly used differentiation protocols that add PPARγ agonists (Lee and Fried, 2014). We hypothesize that such protocols may artificially force BM-Ad progenitors toward a classical white adipocyte differentiation program.

A key finding from our study is the profound alteration of the lipolytic pathway sustained by the strong decrease in MGLL expression, which has never been reported for other forms of AT. Resistance to β-adrenergic stimulated lipolysis in rodent cBM-Ads (from tail vertebrae) and rBM-Ads (from proximal tibia and femur) has been attributed to a decrease in active phosphorylation of HSL; however, MGLL expression was not investigated in this study (Scheller et al., 2019). Although cell energy status or hormones are known to regulate ATGL and HSL activity, no endogenous signals were reported to influence MGLL activity (Lafontan and Langin, 2009), leading us to speculate that MGLL down-expression in BM-Ads is the most efficient way to inhibit its activity.

Concluding Remarks

Through proteomic and lipidomic analyses on human primary BM-Ads, we have revealed specific markers in a phenotype that serves to refine the identity of BM-Ads. Although these cells morphologically resemble classical SC-Ads, we have discovered that the lipid metabolism of BM-Ads, including the presence of a cholesterol-orientated metabolism, is critically different than that seen with SC-Ads. The altered lipolytic function in human primary BM-Ads, due to a profound downregulation of MGLL expression, underlies the differences in metabolic fitness upon caloric restriction between BM-AT and SC-AT. This specific phenotype, a previously unidentified feature of adipose depots, could explain why BM-AT behaves like a preserved lipid source, except during periods of extreme nutrient deprivation (Abella et al., 2002; Cawthorn et al., 2016). Thus, BM-Ads preserve their TG stores and are not likely to release FFA, but they could be an important source of cholesterol and related metabolites. We suspect that BM-Ads may be different in terms of cholesterol metabolism due to their role in BM hematopoiesis (Naveiras et al., 2009; Oguro, 2019; Zhou et al., 2017).

STAR★METHODS

Detailed methods are provided in the online version of this paper and include the following:

- KEY RESOURCES TABLE
- LEAD CONTACT AND MATERIALS AVAILABILITY
- EXPERIMENTAL MODEL AND SUBJECT DETAILS
- METHOD DETAILS
  - Adipocyte isolation
  - SC-AT and BM-AT confocal microscopy
  - Transmission electron microscopy
  - Confocal microscopy on isolated adipocytes
  - Proteomic analysis
  - Lipidomic analysis
  - Cholesterol content quantification
  - *In vitro* adipogenesis
  - Western blot
  - Lipolysis assay
  - cAMP content quantification
- QUANTIFICATION AND STATISTICAL ANALYSIS
- DATA AND CODE AVAILABILITY

SUPPLEMENTAL INFORMATION

Supplemental Information can be found online at https://doi.org/10.1016/j.celrep.2019.12.089.

ACKNOWLEDGMENTS

This work benefited from the assistance of Stephanie Balor and Vanessa Soldan from the Multiscale Electron Imaging platform (METi) of the Centre de Biologie Intégrative (Toulouse, France). Lipidomic analysis was performed at the Mass Spectrometry Facility of the Beth Israel Deaconess Medical Center (Boston, USA). This work was supported by the "Fondation de France" (contract no. 171352) for running costs and a 2-year post-doctoral fellowship for C.A. D.E. received a post-doctoral fellowship from the Fondation pour la Recherche Médicale (SPF201809007124). This work also benefited from the Toulouse Réseau Imagerie (TRI)-RIO Optical Imaging Platform at the Institute of

were normalized to the quantity of total protein. The histograms represent mean ± SEM; *p < 0.05; **p < 0.01 according to two-way ANOVA followed by Bonferroni post-test.

(G) Glycerol release from *in vitro* differentiated 3T3F442A and OP9 cell lines or human BM-MSCs under basal conditions or after stimulation with isoprenaline. The data are the mean of 3 independent experiments (3 independent donors were used for human BM-MSCs) and were normalized to the total lipid quantity per sample. The histograms represent mean ± SEM; *p < 0.05; **p < 0.01 according to two-way ANOVA followed by Bonferroni post-test.

See also Figure S4.

Pharmacology and Structural Biology (Genotoul, Toulouse, France), supported by grants from the Région Midi-Pyrénées (contrat de projets état-région), the Grand Toulouse community, the Association pour la Recherche sur le Cancer (Equipement 8505), the CNRS, and the European Union through the Fonds Européen de Développement Régional program. We thank Life Science Editors for editorial assistance.

AUTHOR CONTRIBUTIONS

N.R. set up the conditions for harvesting BM-AT and SC-AT in close collaboration with C.A. and D.E. and supervised the samples collection. C.A., D.E., and M.M. handled the AT samples and isolated adipocytes. D.E. performed the transmission electron microscopy (with the help of the METi platform) and the immunofluorescence experiments as well as image data analysis. C.A. performed sample preparation for proteomic and lipidomic studies, western blot, cell culture (with the help of M.M.), and the lipolysis experiments. J.C. performed the isolation of human BM-MSC. K.C. performed the proteomics studies under the supervision of O.S. D.E. and C.A. conducted analysis of lipidomic (with the help of P.V.) and proteomic data under the supervision of J.S.I. C.A., D.E., P.V., O.S., and C.M. analyzed the data. C.A., D.E., and C.M. conceived the idea for this project and wrote the manuscript with significant input from all authors. C.M. supervised the study.

DECLARATION OF INTERESTS

The authors declare no competing interests.

Received: August 1, 2019
Revised: November 19, 2019
Accepted: December 24, 2019
Published: January 28, 2020

REFERENCES

Abella, E., Feliu, E., Granada, I., Millá, F., Oriol, A., Ribera, J.M., Sánchez-Planell, L., Berga, L.I., Reverter, J.C., and Rozman, C. (2002). Bone marrow changes in anorexia nervosa are correlated with the amount of weight loss and not with other clinical findings. Am. J. Clin. Pathol. *118*, 582–588.

Ambrosi, T.H., Scialdone, A., Graja, A., Gohlke, S., Jank, A.M., Bocian, C., Woelk, L., Fan, H., Logan, D.W., Schürmann, A., Saraiva, L.R., and Schulz, T.J. (2017). Adipocyte accumulation in the bone marrow during obesity and aging impairs stem cell-based hematopoietic and bone regeneration. Cell Stem Cell *20*, 771–784.

Bartelt, A., and Heeren, J. (2014). Adipose tissue browning and metabolic health. Nat. Rev. Endocrinol. *10*, 24–36.

Bathija, A., Davis, S., and Trubowitz, S. (1979). Bone marrow adipose tissue: response to acute starvation. Am. J. Hematol. *6*, 191–198.

Bredella, M.A., Torriani, M., Ghomi, R.H., Thomas, B.J., Brick, D.J., Gerweck, A.V., Rosen, C.J., Klibanski, A., and Miller, K.K. (2011). Vertebral bone marrow fat is positively associated with visceral fat and inversely associated with IGF-1 in obese women. Obesity (Silver Spring) *19*, 49–53.

Breitkopf, S.B., Ricoult, S.J.H., Yuan, M., Xu, Y., Peake, D.A., Manning, B.D., and Asara, J.M. (2017). A relative quantitative positive/negative ion switching method for untargeted lipidomics via high resolution LC-MS/MS from any biological source. Metabolomics *13*, 30.

Cawthorn, W.P., Scheller, E.L., Learman, B.S., Parlee, S.D., Simon, B.R., Mori, H., Ning, X., Bree, A.J., Schell, B., Broome, D.T., et al. (2014). Bone marrow adipose tissue is an endocrine organ that contributes to increased circulating adiponectin during caloric restriction. Cell Metab. *20*, 368–375.

Cawthorn, W.P., Scheller, E.L., Parlee, S.D., Pham, H.A., Learman, B.S., Redshaw, C.M.H., Sulston, R.J., Burr, A.A., Das, A.K., Simon, B.R., et al. (2016). Expansion of bone marrow adipose tissue during caloric restriction is associated with increased circulating glucocorticoids and not with hypoleptinemia. Endocrinology *157*, 508–521.

Cinti, S. (2001). The adipose organ: morphological perspectives of adipose tissues. Proc. Nutr. Soc. *60*, 319–328.

Corre, J., Mahtouk, K., Attal, M., Gadelorge, M., Huynh, A., Fleury-Cappellesso, S., Danho, C., Laharrague, P., Klein, B., Rème, T., and Bourin, P. (2007). Bone marrow mesenchymal stem cells are abnormal in multiple myeloma. Leukemia *21*, 1079–1088.

Devlin, M.J., Cloutier, A.M., Thomas, N.A., Panus, D.A., Lotinun, S., Pinz, I., Baron, R., Rosen, C.J., and Bouxsein, M.L. (2010). Caloric restriction leads to high marrow adiposity and low bone mass in growing mice. J. Bone Miner. Res. *25*, 2078–2088.

Diedrich, J.D., Rajagurubandara, E., Herroon, M.K., Mahapatra, G., Hüttemann, M., and Podgorski, I. (2016). Bone marrow adipocytes promote the Warburg phenotype in metastatic prostate tumors via HIF-1α activation. Oncotarget *7*, 64854–64877.

Dirat, B., Bochet, L., Dabek, M., Daviaud, D., Dauvillier, S., Majed, B., Wang, Y.Y., Meulle, A., Salles, B., Le Gonidec, S., et al. (2011). Cancer-associated adipocytes exhibit an activated phenotype and contribute to breast cancer invasion. Cancer Res. *71*, 2455–2465.

Doucette, C.R., Horowitz, M.C., Berry, R., MacDougald, O.A., Anunciado-Koza, R., Koza, R.A., and Rosen, C.J. (2015). A high fat diet increases bone marrow adipose tissue (MAT) but does not alter trabecular or cortical bone mass in C57BL/6J mice. J. Cell. Physiol. *230*, 2032–2037.

Fasshauer, M., and Blüher, M. (2015). Adipokines in health and disease. Trends Pharmacol. Sci. *36*, 461–470.

Ghali, O., Al Rassy, N., Hardouin, P., and Chauveau, C. (2016). Increased bone marrow adiposity in a context of energy deficit: the tip of the iceberg? Front. Endocrinol. (Lausanne) *7*, 125.

Hardaway, A.L., Herroon, M.K., Rajagurubandara, E., and Podgorski, I. (2015). Marrow adipocyte-derived CXCL1 and CXCL2 contribute to osteolysis in metastatic prostate cancer. Clin. Exp. Metastasis *32*, 353–368.

Herroon, M.K., Rajagurubandara, E., Hardaway, A.L., Powell, K., Turchick, A., Feldmann, D., and Podgorski, I. (2013). Bone marrow adipocytes promote tumor growth in bone via FABP4-dependent mechanisms. Oncotarget *4*, 2108–2123.

Hindorf, C., Glatting, G., Chiesa, C., Lindén, O., and Flux, G.; EANM Dosimetry Committee (2010). EANM Dosimetry Committee guidelines for bone marrow and whole-body dosimetry. Eur. J. Nucl. Med. Mol. Imaging *37*, 1238–1250.

Justesen, J., Stenderup, K., Ebbesen, E.N., Mosekilde, L., Steiniche, T., and Kassem, M. (2001). Adipocyte tissue volume in bone marrow is increased with aging and in patients with osteoporosis. Biogerontology *2*, 165–171.

Karlsson, M., Reue, K., Xia, Y.R., Lusis, A.J., Langin, D., Tornqvist, H., and Holm, C. (2001). Exon-intron organization and chromosomal localization of the mouse monoglyceride lipase gene. Gene *272*, 11–18.

Kim, S.H., Cho, K.W., Choi, H.S., Park, S.J., Rhee, Y., Jung, H.S., and Lim, S.K. (2009). The forkhead transcription factor Foxc2 stimulates osteoblast differentiation. Biochem. Biophys. Res. Commun. *386*, 532–536.

Krings, A., Rahman, S., Huang, S., Lu, Y., Czernik, P.J., and Lecka-Czernik, B. (2012). Bone marrow fat has brown adipose tissue characteristics, which are attenuated with aging and diabetes. Bone *50*, 546–552.

Lafontan, M., and Langin, D. (2009). Lipolysis and lipid mobilization in human adipose tissue. Prog. Lipid Res. *48*, 275–297.

Lê, S., Josse, J., and Husson, F. (2008). FactoMineR: an R package for multivariate analysis. J. Stat. Softw. *25*, 1–18.

Lee, M.J., and Fried, S.K. (2014). Optimal protocol for the differentiation and metabolic analysis of human adipose stromal cells. Methods Enzymol. *538*, 49–65.

Leitner, B.P., Huang, S., Brychta, R.J., Duckworth, C.J., Baskin, A.S., McGehee, S., Tal, I., Dieckmann, W., Gupta, G., Kolodny, G.M., et al. (2017). Mapping of human brown adipose tissue in lean and obese young men. Proc. Natl. Acad. Sci. USA *114*, 8649–8654.

Litvinov, D.Y., Savushkin, E.V., and Dergunov, A.D. (2018). Intracellular and plasma membrane events in cholesterol transport and homeostasis. J. Lipids *2018*, 3965054.

Liu, Z., Xu, J., He, J., Liu, H., Lin, P., Wan, X., Navone, N.M., Tong, Q., Kwak, L.W., Orlowski, R.Z., and Yang, J. (2015). Mature adipocytes in bone marrow protect myeloma cells against chemotherapy through autophagy activation. Oncotarget *6*, 34329–34341.

Mattiucci, D., Maurizi, G., Izzi, V., Cenci, L., Ciarlantini, M., Mancini, S., Mensà, E., Pascarella, R., Vivarelli, M., Olivieri, A., et al. (2018). Bone marrow adipocytes support hematopoietic stem cell survival. J. Cell. Physiol. *233*, 1500–1511.

Meulle, A., Salles, B., Daviaud, D., Valet, P., and Muller, C. (2008). Positive regulation of DNA double strand break repair activity during differentiation of long life span cells: the example of adipogenesis. PLoS ONE *3*, e3345.

Naveiras, O., Nardi, V., Wenzel, P.L., Hauschka, P.V., Fahey, F., and Daley, G.Q. (2009). Bone-marrow adipocytes as negative regulators of the haematopoietic microenvironment. Nature *460*, 259–263.

Nedergaard, J., Bengtsson, T., and Cannon, B. (2007). Unexpected evidence for active brown adipose tissue in adult humans. Am. J. Physiol. Endocrinol. Metab. *293*, E444–E452.

Nishikata, I., Nakahata, S., Saito, Y., Kaneda, K., Ichihara, E., Yamakawa, N., and Morishita, K. (2011). Sumoylation of MEL1S at lysine 568 and its interaction with CtBP facilitates its repressor activity and the blockade of G-CSF-induced myeloid differentiation. Oncogene *30*, 4194–4207.

Nomura, D.K., Long, J.Z., Niessen, S., Hoover, H.S., Ng, S.W., and Cravatt, B.F. (2010). Monoacylglycerol lipase regulates a fatty acid network that promotes cancer pathogenesis. Cell *140*, 49–61.

Oguro, H. (2019). The roles of cholesterol and its metabolites in normal and malignant hematopoiesis. Front. Endocrinol. (Lausanne) *10*, 204.

Prentice, K.J., Saksi, J., and Hotamisligil, G.S. (2019). Adipokine FABP4 integrates energy stores and counterregulatory metabolic responses. J. Lipid Res. *60*, 734–740.

Ritchie, M.E., Phipson, B., Wu, D., Hu, Y., Law, C.W., Shi, W., and Smyth, G.K. (2015). limma powers differential expression analyses for RNA-sequencing and microarray studies. Nucleic Acids Res. *43*, e47.

Robles, H., Park, S., Joens, M.S., Fitzpatrick, J.A.J., Craft, C.S., and Scheller, E.L. (2019). Characterization of the bone marrow adipocyte niche with three-dimensional electron microscopy. Bone *118*, 89–98.

Scheller, E.L., and Rosen, C.J. (2014). What's the matter with MAT? Marrow adipose tissue, metabolism, and skeletal health. Ann. N Y Acad. Sci. *1311*, 14–30.

Scheller, E.L., Doucette, C.R., Learman, B.S., Cawthorn, W.P., Khandaker, S., Schell, B., Wu, B., Ding, S.Y., Bredella, M.A., Fazeli, P.K., et al. (2015). Region-specific variation in the properties of skeletal adipocytes reveals regulated and constitutive marrow adipose tissues. Nat. Commun. *6*, 7808.

Scheller, E.L., Cawthorn, W.P., Burr, A.A., Horowitz, M.C., and MacDougald, O.A. (2016). Marrow adipose tissue: trimming the fat. Trends Endocrinol. Metab. *27*, 392–403.

Scheller, E.L., Khandaker, S., Learman, B.S., Cawthorn, W.P., Anderson, L.M., Pham, H.A., Robles, H., Wang, Z., Li, Z., Parlee, S.D., et al. (2019). Bone marrow adipocytes resist lipolysis and remodeling in response to β-adrenergic stimulation. Bone *118*, 32–41.

Schreibman, P.H., and Dell, R.B. (1975). Human adipocyte cholesterol. Concentration, localization, synthesis, and turnover. J. Clin. Invest. *55*, 986–993.

Shafat, M.S., Oellerich, T., Mohr, S., Robinson, S.D., Edwards, D.R., Marlein, C.R., Piddock, R.E., Fenech, M., Zaitseva, L., Abdul-Aziz, A., et al. (2017). Leukemic blasts program bone marrow adipocytes to generate a protumoral microenvironment. Blood *129*, 1320–1332.

Szklarczyk, D., Gable, A.L., Lyon, D., Junge, A., Wyder, S., Huerta-Cepas, J., Simonovic, M., Doncheva, N.T., Morris, J.H., Bork, P., et al. (2019). STRING v11: protein-protein association networks with increased coverage, supporting functional discovery in genome-wide experimental datasets. Nucleic Acids Res. *47* (*D1*), D607–D613.

Tabe, Y., Yamamoto, S., Saitoh, K., Sekihara, K., Monma, N., Ikeo, K., Mogushi, K., Shikami, M., Ruvolo, V., Ishizawa, J., et al. (2017). Bone marrow adipocytes facilitate fatty acid oxidation activating AMPK and a transcriptional network supporting survival of acute monocytic leukemia cells. Cancer Res. *77*, 1453–1464.

Taschler, U., Radner, F.P., Heier, C., Schreiber, R., Schweiger, M., Schoiswohl, G., Preiss-Landl, K., Jaeger, D., Reiter, B., Koefeler, H.C., et al. (2011). Monoglyceride lipase deficiency in mice impairs lipolysis and attenuates diet-induced insulin resistance. J. Biol. Chem. *286*, 17467–17477.

Tavassoli, M. (1974). Differential response of bone marrow and extramedullary adipose cells to starvation. Experientia *30*, 424–425.

Vogel, C., and Marcotte, E.M. (2012). Insights into the regulation of protein abundance from proteomic and transcriptomic analyses. Nat. Rev. Genet. *13*, 227–232.

Wen, P.C., Mahinthichaichan, P., Trebesch, N., Jiang, T., Zhao, Z., Shinn, E., Wang, Y., Shekhar, M., Kapoor, K., Chan, C.K., and Tajkhorshid, E. (2018). Microscopic view of lipids and their diverse biological functions. Curr. Opin. Struct. Biol. *51*, 177–186.

Wolins, N.E., Quaynor, B.K., Skinner, J.R., Tzekov, A., Park, C., Choi, K., and Bickel, P.E. (2006). OP9 mouse stromal cells rapidly differentiate into adipocytes: characterization of a useful new model of adipogenesis. J. Lipid Res. *47*, 450–460.

Yeung, D.K.W., Griffith, J.F., Antonio, G.E., Lee, F.K.H., Woo, J., and Leung, P.C. (2005). Osteoporosis is associated with increased marrow fat content and decreased marrow fat unsaturation: a proton MR spectroscopy study. J. Magn. Reson. Imaging *22*, 279–285.

Zechner, R. (2015). FAT FLUX: enzymes, regulators, and pathophysiology of intracellular lipolysis. EMBO Mol. Med. *7*, 359–362.

Zhang, B., Wang, J., Wang, X., Zhu, J., Liu, Q., Shi, Z., Chambers, M.C., Zimmerman, L.J., Shaddox, K.F., Kim, S., et al.; NCI CPTAC (2014). Proteogenomic characterization of human colon and rectal cancer. Nature *513*, 382–387.

Zhao, S., Mugabo, Y., Ballentine, G., Attane, C., Iglesias, J., Poursharifi, P., Zhang, D., Nguyen, T.A., Erb, H., Prentki, R., et al. (2016). α/β-hydrolase domain 6 deletion induces adipose browning and prevents obesity and type 2 diabetes. Cell Rep. *14*, 2872–2888.

Zhou, B.O., Yu, H., Yue, R., Zhao, Z., Rios, J.J., Naveiras, O., and Morrison, S.J. (2017). Bone marrow adipocytes promote the regeneration of stem cells and haematopoiesis by secreting SCF. Nat. Cell Biol. *19*, 891–903.

Zwick, R.K., Guerrero-Juarez, C.F., Horsley, V., and Plikus, M.V. (2018). Anatomical, physiological, and functional diversity of adipose tissue. Cell Metab. *27*, 68–83.

STAR★METHODS

KEY RESOURCES TABLE

REAGENT or RESOURCE	SOURCE	IDENTIFIER
Antibodies		
Rabbit polyclonal antibody anti ATGL	Cell signaling Technology	CAT# 2138S;RRID: AB_2167955
Rabbit polyclonal antibody anti HSL	Cell signaling Technology	CAT# 4107S; RRID: AB_2296900
Rabbit polyclonal antibody anti MGLL	Santa Cruz Biotechnology	CAT# sc134789; RRID: AB_10610918
Mouse monoclonal antibody anti β-Actin	Sigma Aldrich	CAT# A5441; RRID: AB_476744
Goat anti mouse, HRP conjugated	Santa Cruz Biotechnology	CAT# sc2031; RRID: AB_631737
Mouse anti Rabbit, HRP conjugated	Santa Cruz Biotechnology	CAT# sc2357; RRID: AB_628497
Mouse monoclonal antibody anti Perilipin-1	Acris Biosystem	CAT# AM09128SU-N; RRID: AB_10649872
Secondary antibody coupled with CF488 dye	Biotium	CAT# 20014; RRID: AB_10853131
Biological Samples		
Bone marrow and subcutaneous adipose tissue	Orthopedic Surgery and Traumatology Department of the Hospital Pierre Paul Riquet (Toulouse, France)	N/A
Human BM-MSC	University Cancer Institute Toulouse (Jill Corre)	N/A
Chemicals, Peptides, and Recombinant Proteins		
Krebs ringer bicarbonate buffer	Sigma Aldrich	K4002
HEPES	Sigma Aldrich	H3375
Collagenase (lot: 107M4042V)	Sigma Aldrich	C6885-500MG
BSA	Sigma Aldrich	A7030
Cell Strainer 200 μm	Pluriselect	43-50200
Cell Strainer 100 μm	Greiner Bio-One	542000
Paraformaldehyde	Electron Microscopy Sciences	15714
Triton X-100	Sigma Aldrich	T9284
PBS	Thermo Fisher scientific	14190-144
Rhodamine coupled phalloidin	Thermo Fisher scientific	R415
TOPRO3® iodide	Thermo Fisher scientific	T3605
BODIPY 493/503	Thermo Fisher scientific	D3922
Tween 20	Euromedex	2001-B
Glutaraldehyde	Electron Microscopy Sciences	16320
Uranyl acetate	Electron Microscopy Sciences	22400
Reynolds lead citrate	Chromalys	N/A
EMBed-812 resin	Electron Microscopy Sciences	14900
Fibrinogen from bovine plasma	Sigma Aldrich	F8630
Thrombin	Sigma Aldrich	T6634
NaCl	Sigma Aldrich	S7653
$CaCl_2$	Sigma Aldrich	1023820250
Methanol	Sigma Aldrich	179957
Methyl tert-butyl ether	Sigma Aldrich	306975-1L
DTT	Sigma Aldrich	D9163
Glycerol	Euromedex	56-81-5
SDS	Euromedex	EU0660-B
Bromophenol blue	Sigma Aldrich	B0126
Iodoacetamide	Sigma Aldrich	I6125
Coomassie blue	Cliniscience	GEN-QS-STAIN

(*Continued on next page*)

Continued

REAGENT or RESOURCE	SOURCE	IDENTIFIER
Ammonium bicarbonate buffer	Sigma Aldrich	09830
Sequencing grade Modified Trypsin	Promega	V5111
Formic acid	Fluka	94318
Acetonitril Optima LC-MS grade	Fisher Chemical	A955-212
Trifluoro acetic acid	Sigma Aldrich	74564
Isopropanol	Sigma Aldrich	33539-2
MEM alpha	Thermo Fisher scientific	12561
RPMI 1640	Thermo Fisher scientific	61870-010
Fetal Bovine Seru	Thermo Fisher scientific	11573397
Penicillin/ streptomycin	Thermo Fisher scientific	15140-122
Knock-out serum	Invitrogen	10828-028
StemMACS AdipoDiff Media	Miltenyi	130-091-677
4–15% Mini-PROTEAN® TGX gels	Biorad	4568084
ECL prime western blotting detection reagent	Sigma Aldrich	GERPN2232
Protein ladder	Thermo Fisher scientific	26616
TG 10X	Euromedex	EU0550
Isoproterenol hydrochloride	Sigma Aldrich	I6504
Forskolin	Sigma Aldrich	F6886
Heptane	Sigma Aldrich	246654
H_2SO_4	Sigma Aldrich	339741
Tris	Euromedex	200923-A
EDTA	Sigma Aldrich	ED2SS
Critical Commercial Assays		
Free Glycerol Reagent	Sigma Aldrich	F6428
Triglyceride Reagent	Sigma- F6428	T2449
NEFA HR2 - R1	Wako diagnostic	W1W434-91795
NEFA HR2 - R2	Wako diagnostic	W1W436-91995
DC Protein assay kit	Biorad	5000111
Cholesterol/ Cholesteryl Ester Assay Kit	Abcam	ab65359
cAMP complete ELISA kit	Enzo	ADI-900-163
Deposited Data		
Proteomic dataset	This paper	ProteomeXchange: PXD016322
Experimental Models: Cell Lines		
3T3 F442A	ECACC	00070654
OP9	ATCC	CRL-2749
Software and Algorithms		
ChemiDoc XRS+ System		N/A
Graphpad Prism 5	https://www.graphpad.com	N/A
Gene analytics (GeneCards Suite)	https://geneanalytics.genecards.org	N/A
ImageJ software	https://imagej.nih.gov/ij	N/A
Image lab (v5.2.1)	Bio-Rad	N/A
Imaris software (v9.2)	Bitplane	N/A
XCalibur software		N/A
MaxQuant software (v1.6.3.4)		N/A
Swissprot protein database (UniProtKB/Swiss-Prot Knowledgebase release 2018_02).		N/A
FactomineR package (v1.42) within R (v3.6)	Lê et al., 2008	N/A
Limma package (v3.40.2)	Ritchie et al., 2015	N/A

(*Continued on next page*)

Continued

REAGENT or RESOURCE	SOURCE	IDENTIFIER
gplots package (v3.0.1.1)	CRAN: https://cran.r-project.org/web/packages/gplots/index.html	N/A
String database (v11)	Szklarczyk et al., 2019	N/A
Other		
Zeiss LSM 710 confocal microscope	Zeiss	N/A
μQuant spectrophotometer	BioTek Instruments	N/A
ChemiDoc Imaging System	Biorad	N/A
Jeol JEM-1400 transmission electron microscope	JEOL Inc	N/A
Gatan Orius digital camera	Gatan Inc	N/A
UltiMate 3000 RSLCnano system	ThermoFisher Scientific	ULTIM3000RSLCNANO
Q-Exactive Plus mass spectrometer	ThermoFisher Scientific	IQLAAEGAAPFALGMBDK
C-18 precolumn (300 μm ID x 5 mm)	Thermo Fisher	160454
Analytical C-18 column (75 μm ID x 15 cm)	Cluzeau	3PLUS120
Precellys evolution and cryolys	Bertin instruments	N/A

LEAD CONTACT AND MATERIALS AVAILABILITY

Further information and requests for resources and reagents should be directed to Catherine Muller (muller@ipbs.fr) upon reasonable request. This study did not generate new unique reagents.

EXPERIMENTAL MODEL AND SUBJECT DETAILS

Paired subcutaneous (SC-AT) and bone marrow adipose tissue (BM-AT) were harvested from patients undergoing hip surgery at the Orthopedic Surgery and Traumatology Department of the Hospital Pierre Paul Riquet (Toulouse, France). All patients gave informed consent and the samples were obtained according to national ethics committee rules (authorization DC-2017-2914). Briefly, during total hip replacement surgery, after skin incision and maximus gluteus muscle and external rotator dissection, osteotomy of the femoral neck was performed allowing access to the intramedullary canal. While broaching the canal, BM-AT was aspirated cautiously with a soft cannula in the femoral proximal metaphysis and diaphysis before prosthesis placement. All procedures were performed using the same posterior approach. SC-AT were harvested using a surgical blade at the incision site in the gluteal region. The samples were immediately placed in 37°C pre-warmed KRBHA (Krebs Ringer Buffer HEPES Albumin buffer) corresponding to Krebs Ringer buffer (Sigma-Aldrich) supplemented with 100mM HEPES (Sigma-Aldrich) and 0.5% FFA-free bovine serum albumin (BSA) (Sigma-Aldrich) and rapidly transferred to the laboratory (within 1h) where they were processed. BM-AT sharing the same macroscopic aspects, compared to SC-AT, were dissected from areas rich in hematopoietic cells (red marrow). For all experiments, 33 independent samples were obtained from 18 men and 15 women (mean age: 66.9 ± 2.4 and mean body mass index (BMI): 27.3 ± 0.6 kg/m^2).

METHOD DETAILS

Adipocyte isolation

SC-AT and BM-AT were rinsed several times in KRBHA prior to digestion with collagenase (250 UI / mL diluted in calcium and magnesium free PBS supplemented with 2% FFA-free BSA. After 30 min digestion at 37°C under constant shaking, samples were filtered with 100 and 200μm cell strainers (for BM-AT and SC-AT respectively) to remove cellular debris, undigested fragments and bone trabeculae. The mean size of isolated BM-Ad and SC-Ad populations was not statistically different (95 ± 6μm for SC-Ad and 90 ± 7μm for BM-Ad). The cell suspensions were then gently centrifuged for 5 min at 200 g at room temperature (RT). Floating adipocytes were collected and rinsed with KRBHA several times to obtain pure adipocyte cell suspensions.

Isolated adipocytes were gently homogenized with KRBHA and were seeded onto plastic slides in 5ul drops. Adipocytes in the upper portion of the drop were immobilized with spacers and plastic coverslips. Images from several drops were immediately taken with an upright brightfield microscope (ZEISS Axio Imager 2) and 5x objective (ZEISS 5X EC plan NeoFluar). At least 300 adipocytes from each sample were manually measured with imageJ.

SC-AT and BM-AT confocal microscopy

Pieces of 0.5 cm^2 whole SC-AT and BM-AT were fixed overnight with a 4% paraformaldehyde (PFA) solution from Electron Microscopy Sciences, Hatfield, PA, USA (EMS). Fixed tissues were blocked and permeabilized for 1 h at RT in calcium and magnesium free PBS supplemented with 3% BSA and 0.2% Triton X-100 (Sigma Aldrich). Tissues were then incubated overnight with mouse anti

PLIN1 serum (Acris Biosystem) 1:10 in calcium and magnesium free-PBS, 3% BSA, 0.2% Triton X-100. The following day, tissues were rinsed 5 times in PBS 0.05% Tween-20 and incubated for 2 h with a secondary antibody coupled with CF488 dye (Biotium) for PLN1 staining, rhodamine coupled phalloidin and TOPRO3® (Thermo Fisher Scientific, Bremen, Germany) for filamentous actin staining and nuclei staining, respectively. Z stack images were acquired using an LSM 710 confocal microscope with 10X and 40X objectives (Zeiss). Maximum intensity projections were made using ImageJ (NIH) and orthogonal views with Imaris software (v9.2; Bitplane).

Transmission electron microscopy

SC-AT and BM-AT were fixed overnight at 4 °C with 2.5% glutaraldehyde and 2% PFA (EMS) in Cacodylate buffer (0.1M, pH 7.2) and post-fixed at 4°C with 1% OsO4 and 1.5% K3Fe(CN)6 in the same buffer. Samples were treated for 1 h with 1% aqueous uranyl acetate and were then dehydrated in a graded ethanol series and embedded in EMBed-812 resin (EMS). After 48 h of polymerization at 60 °C, ultrathin sections (80 nm thick) were mounted on 75 mesh formvar-carbon coated copper grids. Sections were stained with 2% uranyl acetate (EMS) and 3% Reynolds lead citrate (Chromalys). Grids were examined with a Jeol JEM-1400 transmission electron microscope (JEOL Inc) at 80 kV and images were acquired with a Gatan Orius digital camera (Gatan Inc, Pleasanton, CA, USA).

Confocal microscopy on isolated adipocytes

BM-Ad and SC-Ad were isolated as described above. Immediately after isolation, primary adipocytes were embedded in a fibrin gel to maintain cellular integrity. Briefly, 30μl of isolated adipocytes were gently mixed with 30μl of an 18 μg/mL fibrinogen (Sigma-Aldrich) solution in 0.9% NaCl buffer and 30μl of thrombin, 3 units in 30μl of $CaCl_2$ solution (Sigma-Aldrich). Gel polymerization rapidly occurred at 37°C. Gels containing primary adipocytes were fixed in 4% PFA for 1h and incubated with 10 ng/mL of Bodipy® 493/503, rhodamine coupled phalloidin and TOPRO3 (Thermo Fisher Scientific). Samples were examined using an LSM 710 confocal microscope with a 40X objective (Zeiss). Maximum intensity projection was performed using ImageJ.

Proteomic analysis

For proteomic and lipidomic studies, 4 samples were used (2 men and 2 women, mean age: 67 ± 7. 4 years; mean BMI: 26.5 ± 3.1 kg/m^2). After 3 washes with PBS, isolated adipocytes (400 μl) were mixed 1.5 mL methanol in glass tubes. Sample mixtures were then incubated with 5 mL of methyl tert-butyl ether (MTBE; Sigma-Aldrich) for 1h at RT under gently shaking. After adding 1.2 mL of water, samples were centrifuged for 10 min at 1000 g. The lipid containing upper phase was transferred to a new glass tube. The lower phase was re-extracted with 2 volumes of MTBE:methanol:water (10:3:2.5) and samples were centrifuged for 10 min at 1000 g before proteomic analyses. The upper phase was collected, combined with the one collected after the first extraction and kept at −80°C for lipidomic analysis (see below). The lower phase was centrifuged for 10 min at 5000 g at RT and the pellet (containing proteins) was washed 2 times with PBS to remove solvents. Pellets were then resuspended with PBS 2% SDS, sonicated for 20 s and protein concentration was determined with the DC Protein Assay kit (Bio-Rad). For each sample, 15μg of protein was reduced with modified Laemmli buffer (40 mM Tris pH 6.8, 2% SDS, 10% glycerol, 25mM DTT and 0.01% bromophenol blue) for 15 min at 65°C and alkylated by the addition of 90mM iodoacetamide for 30 min at RT in the dark. Protein samples were loaded on a 1D SDS-PAGE gel (0.15 × 8 cm) and the electrophoretic migration was stopped as soon as the proteins entered the separating gel, in order to isolate all proteins in a single gel band (stained with Coomassie blue). The corresponding gel slices were excised and washed with 100 mM ammonium bicarbonate buffer. Proteins were in-gel digested using 0.6 μg of modified sequencing grade trypsin (Promega) in 50 mM ammonium bicarbonate overnight at 37°C. The resulting peptides were extracted in 50 mM ammonium bicarbonate followed by 10% formic acid/acetonitrile (1/1 v/v). The peptidic fractions were dried under speed-vacuum and resuspended with 5% acetonitrile and 0.05% trifluoroacetic acid (TFA) for MS analysis.

Peptides were analyzed by nanoLC-MS/MS using an UltiMate 3000 RSLCnano system coupled to a Q-Exactive Plus mass spectrometer (Thermo Fisher Scientific). Five μL of each sample was loaded onto a C-18 precolumn (300 μm ID x 5 mm, Thermo Fisher) in a solvent consisting of 5% acetonitrile and 0.05% TFA with a flow rate of 20 μL/min. After 5 min of desalting, the precolumn was switched online with the analytical C-18 column (75 μm ID x 15 cm, Reprosil C18) equilibrated in 95% solvent A (5% acetonitrile, 0.2% formic acid) and 5% solvent B (80% acetonitrile, 0.2% formic acid). Peptides were eluted using a 5 to 50% gradient of solvent B over 300 min at a flow rate of 300 nL/min. The Q-Exactive Plus was operated in a data-dependent acquisition mode with the XCalibur software. MS survey scans were acquired in the Orbitrap on the 350-1500 m/z range with the resolution set to a value of 70000. The 10 most intense ions per survey scan were selected for HCD fragmentation and the resulting fragments were analyzed in the Orbitrap with the resolution set to a value of 17500. Dynamic exclusion was employed within 30 s to prevent repetitive selection of the same peptide. Duplicate technical LC-MS measurements were performed for each sample.

Raw mass spectrometry files were processed and quantitated with the MaxQuant software (version 1.6.3.4) with database search using the Andromeda search engine. Data were searched against human entries from the Swissprot protein database (UniProtKB/Swiss-Prot Knowledgebase release 2018_02). Carbamidomethylation of cysteines was set as a fixed modification whereas oxidation of methionine and protein N-terminal acetylation were set as variable modifications. Specificity of trypsin digestion was set for cleavage after K or R, and up to two missed trypsin cleavage sites were allowed. The precursor mass tolerance was set to 20 ppm for the first search and 4.5 ppm for the main Andromeda database search. The mass tolerance MS/MS mode was set to 0.5 Da. Minimum peptide length was set to seven amino acids, and minimum number of unique peptides was set to one. Andromeda results were

validated by the target-decoy approach using a reverse database with both peptide and protein FDR at 1%. For label-free relative quantification of the samples, the "match between runs" option of MaxQuant was enabled with a time window of 0.7min, to allow cross-assignment of MS features detected in the different runs. The "label free quantification" (LFQ) metric from the MaxQuant "protein group.txt" output was used to quantify proteins. Missing protein intensity values were replaced by a constant noise value determined independently for each sample as the lowest value of the total protein population. Only proteins identified in at least three samples in the same location (i.e., SC-Ad or BM-Ad) were considered to be robustly detected and used for statistical and bioinformatic analyses.

Protein involved in lipid and glucose metabolism were selected using Gene Analytics software (GeneCards Suite) based on their involvement in the following pathways: Regulation of lipid metabolism, Insulin signaling-generic cascades, Lipoprotein metabolism, Adipogenesis, Regulation of lipid metabolism by Peroxisome proliferator-activated receptor alpha, Glucose / Energy Metabolism, Peroxisomal lipid metabolism, Calcium (Ca), cyclic adenosine monophosphate (cAMP) and Lipid Signaling, Nuclear Receptors in Lipid Metabolism and Toxicity, SREBF (Sterol Regulatory Element Binding Protein) and miR33 in cholesterol and lipid homeostasis, Acyl chain remodeling of Phospho Ethanolamine (PE) Cholesterol and Sphingolipids transport / Distribution to the intracellular membrane compartments, Synthesis of substrates in N-glycan biosynthesis, Synthesis of PhosphatidylCholine (PC), Metabolism of steroid hormones, Glycerophospholipid biosynthesis, Glucose metabolism, Fat digestion and absorption, Regulation of cholesterol biosynthesis by SREBP (Sterol Regulatory Element Binding Protein), cholesterol biosynthesis III (via desmosterol), Cholesterol and Sphingolipids transport / Transport from Golgi and ER to the apical membrane, Aldosterone synthesis and secretion, Citrate cycle (Tricarboxylic Acid (TCA) cycle), Adipocytokine signaling pathway, Sphingolipid metabolism, Fatty acid metabolism, Pyruvate metabolism, Arachidonic acid metabolism, Linoleic acid metabolism, Ceramide Pathway, Sphingolipid signaling pathway, sphingomyelin metabolism/ceramide salvage, Pentose phosphate pathway, Regulation of lipolysis in adipocytes, Mitochondrial Long Chain-Fatty Acid, Beta-Oxidation SuperPath and Fatty acid biosynthesis. Among the 1948 proteins retrieved by the database, we identified 612 proteins that belong to one or more of the above pathways. The LFQ intensity for each identified protein was log2 transformed and used to perform principal component analysis with the FactomineR package (v1.42) within R (v3.6). The statistical analysis of differentially expressed proteins was performed with the limma package (v3.40.2) where a linear model was fit using a two group (BM-Ad and SC-Ad) design matrix followed by empirical Bayes moderation (see Table S1). Protein expression was considered significantly different if the p value was less than 0.05.

Pathway enrichment analysis was performed with Gene Analytics (GeneCards) using official gene symbols. Heatmaps with hierarchical clustering of samples were made with the gplots package (v3.0.1.1). Network analyses were performed with the String database (v11) using the following queries: Regulation of lipolysis in adipocytes, statin and cholesterol biosynthesis and lipoprotein metabolism. Confidence scores above 0.8 were considered as significant. Protein-protein interaction (PPI) networks were created using cytoscape (v3.7.1). Nodes were color-coded according to the log2 fold-change of protein expression detected by LC-MS/MS in BM-Ad compared to SC-Ad. Node sizes were attributed according to the p value of differential expression analysis from the linear model used for differential expression analysis. Edges, which represent the different types of interactions, are color-coded: red for experimentally determined physical and functional interactions with a score above 0.3, blue for coexpression, which reflects whether or not the protein is co-expressed in the same biological model, and gray for known interactions from curated databases with a confidence score above 0.8 (see https://STRING-db.org for additional information).

Lipidomic analysis

One ml of the lipid phase, extracted with MTBE as described above, was evaporated under a nitrogen stream. Dried samples were sent to the Harvard mass spectrometry core and were analyzed by their untargeted lipidomics profiling platform. Lipids were resuspended with 100μl of 1:1 LC/MS grade isopropanol:acetonitrile methanol and 5 μl was injected onto the LC-MS/MS. Data acquisition was performed as previously described (Breitkopf et al., 2017). Briefly, each peak area was calculated in both positive and negative ionization mode. Peaks structurally resolving to the same lipid species were summed when obtained from the same ionization. Only lipid species detected in at least 3 samples from the same location were considered as robustly detected and used for the analysis. Missing values were imputed as the first percentile of the entire dataset. Values were log2 transformed and normalized with the function "Normalize Between Arrays" from the limma package (v3.40.2) within R (v3.6). Lipid species belonging to the same class were summed to obtain relative abundances and the log2 fold change of signal intensities for each class were calculated in order to compare lipid classes between adipocyte locations.

Cholesterol content quantification

The cholesterol content of isolated adipocytes was measured using a cholesterol assay kit (Abcam- ab65390) according to manufacturer recommendations. Briefly, lipids were extracted from isolated adipocytes using MTBE as described above. Free cholesterol and total cholesterol were sequentially quantified using colorimetric methods. Optical density was determined at 570 nm with μ-quant spectrophotometer (BioTek Instruments).

In vitro adipogenesis

The pre-adipocyte 3T3 F442A obtained from ECACC (00070654) were grown and differentiated into adipocytes as previously described (Meulle et al., 2008). OP9 cells were obtained from ATCC (CRL-2749). OP9 cells were seeded at $1x10^5$ cells/well in

6-well plates and cultured for 2 days in MEM alpha supplemented with 20% fetal calf serum (FCS), 125 mg/mL streptomycin and 125 UI/mL penicillin. At 80% confluence, media was replaced with a similar media supplemented with 15% knock-out serum (Invitrogen 10828-028) for 5 days to induce adipogenic differentiation (Wolins et al., 2006). Human BM-MSC were isolated from bone marrow (obtained by sternal puncture) of healthy patients, as previously described (Corre et al., 2007). BM-MSC (passage 1) were seeded at $3x10^5$ cells/well in 6-well plates and cultured for 2 days in MEM alpha supplemented with 10% FCS, 125mg/mL streptomycin and 125UI/mL penicillin. At 80% confluence, media was replaced with StemMACS AdipoDiff Media (Miltenyi 130-091-677) supplemented with 125mg/mL streptomycin and 125UI/mL penicillin to induce adipogenic differentiation over 28 days. Media was changed every 2 to 3 days and cells were grown in a humid atmosphere with 5% CO2 at 37°C. TG content of cells before and at the end of adipogenic differentiation was performed as previously described (Dirat et al., 2011) using a commercial kit (Sigma- F6428).

Western blot

Isolated adipocytes were washed 3 times with PBS and proteins were separated from lipids using MTBE extraction, as described in the proteomic analysis section. Five μg of proteins were reduced with modified Laemmli buffer for 15 minutes at 65°C, loaded on a 4%–10% gradient SDS-PAGE gel (Biorad) and transferred to nitrocellulose membranes. Membranes were blocked with 5% skimmed milk in TBS (20mM Tris, 150mM NaCl) and incubated with appropriate primary antibodies: rabbit polyclonal antibody (pAb) anti ATGL, (1/:1000, ref: 2138, Cell Signaling Technology); rabbit pAb anti HSL (1:1000, ref: 4107, Cell Signaling Technology); rabbit pAb anti MGLL (1:1000, ref: sc134749, Santa Cruz Biotechnology); mouse monoclonal anti β-Actin (1:5000, clone: AC-15, Sigma Aldrich). The membranes were washed with TBS complemented with 0.1% Tween-20 and incubated with HRP conjugated secondary antibodies (1:5000, Santa Cruz Biotechnology). The immunoreactive protein bands were revealed by ECL prime western blotting detection reagent (Ammersham™) and detected using a ChemiDoc Imaging System (Biorad). Densitometry quantification was performed using Image lab software (v5.2.1; Bio-Rad). Signal intensities were normalized to β-Actin.

Lipolysis assay

Isolated adipocytes (50 μl) or AT explants (~50 mg) were incubated with 450 μL KRBHA with or without isoprenaline 1μmol/ L (Sigma Aldrich) or forskolin 10μmol/L (Sigma Aldrich) to evaluate stimulated and basal lipolysis. After 2 h incubation at 37°C under gentle shaking, 200 μL of incubation media was removed and kept to measure glycerol and FFA release using commercial kits (Sigma-F6428 and Wako diagnostic NEFA-HR, respectively). Results were normalized to the total lipid content quantified after Dole extraction. Briefly, isolated adipocytes were lysed by the addition of Dole's Reagent (40:10:1 isopropanol:heptane:H_2SO_4 1N). The upper phase, containing lipids, was extracted again with heptane, evaporated under a nitrogen stream and weighed as dried lipids. For lipolysis experiment on adipocyte-differentiated cell lines (3T3 F442A and OP9) and human BM-MSC, cells were incubated for 3 hours and the results were normalized to TG content. At the end of the incubation, cells were washed with PBS and resuspended in buffer containing 10mM Tris HCL pH 7.5 and 1mM EDTA to quantify TG.

cAMP content quantification

AT explants (~50 mg) were incubated with 450 μL KRBHA with or without 1μmol/ L isoprenaline (Sigma Aldrich) for 30 minutes at 37°C under gentle shaking, At the end of the incubation, explants were rapidly rinsed in PBS and immediately frozen in liquid nitrogen. Frozen AT explants were then homogenized at 4°C in five volume of 0.1 M HCl using a Precellys homogenizer with cryolys cooling system (Bertin instruments). Homogenates were centrifuged for 10 min at 15,000 g and the aqueous phase was transferred to a new tube for cAMP quantification using an ELISA kit (Enzo) according to the manufacturer's instructions.

QUANTIFICATION AND STATISTICAL ANALYSIS

Statistical analyses were performed using Prism v5 (GraphPad Software). Two group comparisons were performed using paired Student's t test and multiple comparisons were performed by two-way ANOVA followed by Bonferroni post-test for n independent experiments. P values were considered significant if lower than 0.05. All the statistical details (statistical tests used, n numbers and data dispersion) can be found in the figure legend.

DATA AND CODE AVAILABILITY

The accession number for the mass spectrometry proteomic data reported in this paper is ProteomeXchange: PXD016322.